reprint

Probing microcavity switching events on the picosecond time scale using quantum dots as a broadband internal fluorescent source

Tobias Sattler,[1] Guilherme Monteiro Torelly,[1,2] Emanuel Peinke,[1] Arthur Gérard,[1] Julien Claudon,[1] Joël Bleuse,[1] Patricia Lustoza Souza,[2] and Jean-Michel Gérard[1, a)]

[1)] *Univ. Grenoble Alpes, CEA, IRIG-PHELIQS, "Nanophysique et semiconducteurs" group, F-38000 Grenoble, France*

[2)] *LabSem-CETUC, Pontifícia Universidade Católica do Rio de Janeiro, 22451-900, Brazil*

(Dated: 20 November 2020)

We report on ultrafast all-optical switching experiments performed on pillar microcavities containing a collection of quantum dots (QDs). Using QDs as a broadband internal light source and a detection set-up based on a streak camera, we track in parallel the frequencies of a large set (>10) of resonant modes of an isolated micropillar, during the entire duration of switching events and with a 2 ps temporal resolution. Being much faster and more convenient than standard approaches based on pump-probe spectroscopy, this method is very well suited for in-depth studies of cavity switching, noticeably in view of applications in the field of quantum photonics. We report as a first demonstrative example an investigation of the switch-on time constant τ_{on} dependence as a function of the pump power and the observation of a remarkably low value of $\tau_{on}(\approx 1.5\,\mathrm{ps})$ for optimized pumping conditions. As a second illustration, we report the observation of a transient lifting of the degeneracy of a polarization-degenerate cavity mode, induced by a non-centrosymmetric injection of free-carriers.

[a)]Electronic mail: jean-michel.gerard@cea.fr; T.S. and G.M.T. equally contributed to this work

I. INTRODUCTION

It is well known that the frequency of the resonant modes of semiconductor microcavities, and thus their optical response, can be changed in a transient and reversible way, through a modification of the refractive index of the constituent material[1,2]. This effect, known as "cavity switching", has been initially implemented in the mid 80's on pillar microcavities, in view of ultrafast all-optical data processing and computing. Nowadays, "cavity switching" induced by the electrical injection of free carriers is widely used on the microsecond time scale for the reconfiguration of integrated photonic circuits[3]. Cavity switching can be achieved in a much faster way through optical modifications of the refractive index. All-optical switching on a sub-ps time scale has been achieved using the electronic Kerr effect[4], and the optical injection of free charge carriers is routinely used to induce cavity switching on the few-ps time scale[1,2,5–9]. Ultrafast all-optical cavity switching encounters renewed interest motivated by its important potential applications in the field of quantum photonics. Cavity switching enables modifying at will the detuning between a mode and an artificial atom such as a quantum dot. It could be used to switch on and off Rabi oscillations in the strong coupling regime, or to control in a dynamic way the magnitude of the Purcell effect[10,11], e.g. to tailor the temporal-envelope of a single photon pulse[12]. Finally, the switching of high-Q microcavities changes the frequency of trapped light as demonstrated in "color change" experiments[6,13]; this effect could be in the future at work in single photon frequency-translators.

In view of such applications, a precise knowledge of the dynamics of cavity switching events is mandatory. Reports of advanced characterization of switching events are rather scarce for the well-known micropillar geometry, which is an essential workhorse of quantum photonics, both for basic CQED experiments[14,15] and for the development of novel devices such as microlasers[15], single photon sources[16–18] or bistable devices[19]. The mainstream approach is ultrafast pump-probe spectroscopy in reflection geometry, which has been used to investigate switching events in planar cavities[2,4,5] and later in micropillars[20]. Despite providing excellent time-resolution, such experiments are relatively slow, which hinders extensive parametric studies. Furthermore, transmission or reflection spectroscopy only permits probing the modes which present a non-zero overlap with the probe beam. As an example, for a Gaussian beam whose waist is matched to the top facet of a pillar microcavity, only

the fundamental mode of the pillar contributes to the reflection or transmission signal[1,21]. Considering now other microcavities such as ring resonators of photonic crystal cavities, information on the switching event has also been obtained as a by-product of color-change experiments. In the (standard) adiabatic regime, the color change indeed faithfully reflects the frequency shift of the resonant cavity mode that has been used to store and convert light[6]. In such experiments, information is obtained for one mode at a time. Finally, information about the dynamic evolution of mode frequencies can also be extracted from photoluminescence experiments on active microcavities containing one or several QDs as shown for single-mode photonic crystal cavities[9,11].

We introduce our experimental approach in section II: a broadband internal light source lights-up all the resonant modes of a cavity prior to the switching event, and a detection set-up combining a grating spectrometer and a streak camera enables tracking the time-dependent frequencies of the resonant modes during the entire switching event with ps-time resolution. Although our method can potentially be used to study any cavity, and noticeably photonic crystal nanocavities, we chose in this work GaAs/AlAs micropillars as a first example. In our experiments, information is simultaneously obtained for a large (>10) set of resonant modes and for all relevant time delays. We highlight in section III the interest of this experimental approach via the study of the on/off switching times for a GaAs/AlAs micropillar as a function of the switching pulse energy. A switch-on time constant as short as 1.5 ps is observed for optimized pumping conditions. We also report in section IV the observation of major transient differential switching effects including the degeneracy lifting of a pillar mode, induced by breaking the rotational pillar symmetry through an asymmetric injection of free-carriers.

II. EXPERIMENTAL APPROACH

We study GaAs/AlAs pillar microcavities which contain a large ensemble of InAs QDs, as described in Ref. 14. Since the mid 90's, embedded QDs have been widely used to probe the frequencies, quality factors and radiation patterns of resonant cavity modes[21–23]. In the spontaneous emission regime, QDs work as independent punctual emitters and light up systematically all cavity modes present within the broad frequency range covered by their inhomogeneously broadened emission line[22]. For the micropillars under study, the diameter

is comprised between 2 and 7 μm and the quality factor Q of the fundamental mode varies between 4000 and 5000.

Our experimental set-up is sketched in Fig.1. The QD-micropillar sample is placed at 4 K inside a He-flow cryostat. The pump beam is delivered by a mode-locked Ti:sapphire laser (200 fs pulse duration, 76 MHz repetition rate) which is both used to excite the QDs and to switch the cavity through the injection of free-carriers in all GaAs sublayers. The pump beam is focused on the top facet of an isolated micropillar by a NA= 0.25 microscope objective. The photoluminescence of the QD-micropillar is collected by the same objective and analyzed spectrally and temporally using a system composed of a Jobin-Yvon Triax320 monochromator and a Hamamatsu C10910 streak camera. This system provides a temporal resolution around 2 ps, combined to a 0.3 meV resolution in the photon energy/frequency domain, close to the limit imposed by the time-energy uncertainty principle. A sub-ps time resolution can also be obtained by using the spectrometer grating in its 0^{th} order diffraction mode.

When QDs are excited through optical injection of electron-hole pairs within the wetting layer or GaAs barrier, their photoluminescence rise time is about 25 ps, due to the delays induced by carrier capture and relaxation[14]. Therefore, when both QD pumping and micropillar switching are both induced by the same pump pulse, one cannot study the switch-on behavior during the first picoseconds after the pulse as shown in previous reports[9,24], because the QD-photoluminescence is too weak. We use for this reason a two-pulses pumping sequence to ensure that the internal light source is bright enough to probe the entire switching event. We use a fibered system to split Ti:sapphire pulses into a weak pulse, which lights-up the QDs but does not induce significant switching, and a stronger one, which is delayed by Δ ps with respect to the first one and switches the cavity. We define γ (resp. $1-\gamma$) the fraction of the pump power that goes into the strong (resp. weak) pulse.

In order to give a better idea of how raw data generated by the streak camera look like, we show in Fig.2, as a first example, an image obtained by switching a 5.3 μm-diameter micropillar. Here, the pump photon energy is 1.57 eV and the diameter of the pump beam is much larger at its waist (10 μm) than the pillar diameter so as to ensure a uniform injection of electron-hole pairs in the GaAs cavity layer. Thanks to the QDs uplighting prior to the switching pulse, the spectral position of the six lowest frequency emission lines of the micropillar is clearly seen before the switching event that is induced around $t = 0$.

We identify the emission lines from a standard modelling[22]. We start with a calculation of the effective indices of the guided modes of a 5.3 μm diameter cylinder in air[25]. Each guided mode m of the cylinder gives rise to a single resonant mode in the micropillar, whose resonance frequency ν_m is given by[22] $\nu_{2D}/\nu_m = n_m^{eff}/n$, where n is the refractive index of undoped GaAs, ν_{2D} the resonance frequency of the planar cavity from which the micropillar has been defined and n_m^{eff} the effective index of the guided mode m. In Fig.2, we use as labels for the pillar modes the usual names[25] HE_{ij} or EH_{ij} of their "parent" guided modes in the GaAs cylinder. Several modes, which are close in frequency, contribute to a common emission line in the micropillar spectrum. The three lower frequency lines appear brighter than the higher frequency ones, since their frequencies are closer to the center of the inhomogeneous distribution of QDs (located at around 1.36 eV).

In this experiment, QDs are most of the time decoupled from any cavity mode. Apart from short transient coupling events with modes, their excitonic population decays on a time scale of the order of 1 ns. Thanks to this relatively slow decay, the QDs can be employed to monitor the entire switching event. This is exemplified in Fig.2, which shows a measurement using the long time-range mode of the streak camera. Due to the uniform modification of the refractive index of GaAs, all modes display the same switching behavior. The second pump pulse induces a sudden blue-shift of the mode frequencies. Here, the switching amplitude is around 1.8 meV, which corresponds to 7 mode linewidths, and the switch-on time (not resolved in this long time range mode) is below 20 ps. Next, all modes relax toward their original frequency due to the recombination of the electron-hole pairs. Here, the relaxation dynamics is close to exponential with a 200 ps time constant after $t = 100$ ps. In this time range, the dynamics is dominated by the non-radiative recombination (NRR) at sidewalls, as shown for similar micropillars in Ref. 20. At short delays after the switch pulse, (0<t<100ps), the density of the electron-hole plasma is higher and the radiative recombination of electron-hole pairs enters into play, which leads to a faster relaxation of the modes. In Fig.2, the time–dependence of the frequency of the fundamental mode HE_{11} is well reproduced by a biexponential curve with time constants 50 ps and 200 ps. The same curve, shifted along the frequency axis by an amount corresponding to the frequency spacing between unswitched pillar modes, describes the behavior of higher order modes. We see that a very similar behavior is observed for all modes thanks to the uniform injection of free carriers. The amplitude of this global blue shift of the modes (≈ 1.8 meV) corresponds to a $\delta n = -4.5.10^{-3}$

change of the refractive index of GaAs at around 1.39 eV.

A streak camera image such as the one shown in Fig.2 is the result of a 20-minutes-long experimental run, including background level acquisition and subtraction. By contrast, several days would be necessary to obtain similar information using pump-probe spectroscopy. The method that is introduced here looks as particularly well suited for performing extensive parametric investigations. In the next sections, we will focus our attention on the ultrafast switch-on behavior of micropillars.

III. PROBING THE SWITCH-ON DYNAMICS ON THE FEW-PS TIMESCALE

Figure 3 shows two streak camera images obtained in a high temporal resolution mode (70 ps time range, 1 ps resolution) from a 3 μm diameter micropillar. Here, the pump photon energy is 1.55 eV. The pump beam diameter at the waist is matched to the micropillar top facet and two different switching pulse energies, 0.5 pJ and 7 pJ, are used. We study the switch-on behavior of the first two unresolved sets of modes of the micropillar, labelled as *Line 1* for the two-fold degenerate fundamental mode HE_{11}, and as *Line 2* for the second set, which comprises non-degenerate modes HE_{01} and EH_{01} and the polarization-degenerate mode HE_{21}. Thanks to the excitation of the QDs by the first pump pulse 200 ps prior to the switching pulse, one can observe *Line 1* and *Line 2* before and during the switching event, induced at around $t = 20$ps. These emission lines are observed at frequencies that remain constant between 0 and 20 ps, and are identical to those of the unswitched micropillar. This confirms that the residual density of electron-hole pairs due to the excitation by the first pulse is small enough to avoid any significant frequency shift of the pillar modes. We can use these frequencies as references to track switching effects.

Important properties of free-carrier switching are deduced from the analysis of Fig.3. As we can track mode frequencies during the switching event, we can probe precisely the dynamics of the physical processes responsible for the blue shift ("switch-on") and for the relaxation ("switch-off") of the modes. Considering *Line 1*, we see that raising the pump power increases (as expected) the magnitude of the frequency shift, and accelerates very significantly the switch-on. Slightly longer switch-on times, albeit still in the few-ps range, are observed for *Line 2*.

As discussed in detail in Ref.26, three effects contribute to changes in the absorption coefficient of the semiconductor (and thus to its refractive index owing to the Kramers-Kronig relations) : bandgap shrinkage related to many-body effects, interband absorption bleaching (IAB) due to state filling in the conduction and valence bands and intraband free carrier absorption (FCA). At plasma densities well above 10^{17}cm^{-3}, which are typically used in free carrier switching experiments such as ours, the dominant effect is IAB, with an additional contribution from FCA. According to Kramers-Kronig relationships, modifications of the absorption coefficient close to the semiconductor bandgap induce larger changes of the refractive index. Although the hot carriers induced by the pump should in principle induce FCA, and some instantaneous change of the refractive index, we do not detect such an effect for P =0.5 pJ in Fig. 3. Our results are fully compatible with a dominant role of IAB. The thermalization and cooling of the electron-hole plasma results in a filling of states at the bottom of the conduction and valence bands and in an increased modification of the refractive index.

To precisely estimate relevant time constants, we have fitted the time-dependence of the line frequencies using a simple rate equation model. We consider that the pump pulse injects free carriers within 0.9 ps into high-energy states, which behave as a reservoir. They relax from this reservoir toward the extrema of the conduction and valence bands with a characteristic time τ_{on}, thereby inducing a change in the absorption and refractive index of GaAs. Free carriers also recombine with a time constant τ_{off}. We assume that the modification of the refractive index -and consequently the shift of the modes- is proportional to the density of relaxed carriers, which is a reasonable approximation for carrier densities above 10^{17}cm^{-3} .[26] We use τ_{on}, τ_{off} and the switching amplitude as fitting parameters. As shown in Fig.3, this elementary model captures adequately the shape of the entire switching event for both small and large switching energies.

We plot in Fig.4 the evolution of τ_{on} as a function of the switching pulse energy P. For *Line 1*, we observe a strong decrease of τ_{on}, from 6 ps for small Ps, down to 1.5-2 ps for the largest Ps. We attribute this effect to enhanced electron scattering at high carrier densities. As cooling of the electron-hole plasma occurs most efficiently through LO-phonon emission, carrier-carrier scattering plays an essential role as it ensures filling high-energy states located more than one LO-phonon energy above the bottom of the band, favoring thermalization mediated by LO-phonons. The slight apparent increase of τ_{on} that is observed

above 6 pJ is an experimental artefact. In this power range, non-linear effects in the optical fibers induce a stretching of the pump pulses from 200 fs to about 2 ps and a smoothing of the switch-on behavior. Quite remarkably, we observe values of τ_{on} as short as 1.5 ps under optimum pumping conditions (here $P \approx 4$ pJ). This value is significantly shorter than previously published data extracted from pump-probe experiments using a two-photon excitation scheme (e.g. 6 ps in Ref. 5). By contrast, our results agree well with prior studies of carrier relaxation after excitation by a femtosecond pulse at 1.55 eV , which reveal a drastic evolution of GaAs absorption around its bandgap during the first picosecond[27]. It is likely that two-photon excitation well above the gap, as used in Ref. 5, creates a hotter electron-hole plasma than the one-photon pumping scheme that is used in our study, which delays the cooling of the electron-hole plasma.

Considering now *Line 2*, we observe a slightly longer switch-on time. As we have matched the pump beam size to that of the top facet of the micropillar, the electron-hole plasma density is larger around the micropillar axis, and a transverse diffusion of the charge carriers occurs during and after the cooling. As can be seen in Fig.5 all four modes contributing to *Line 2* possess a node at the pillar axis. Therefore, their best overlap with the free carriers is obtained once some lateral diffusion has occurred, which induces a further delay for *Line 2* on top of the switch-on time constant of *Line 1*. As shown in Ref. 20, such behavioral differences between *Line 1* and *Line 2* can be modelled in a quantitative way when the ambipolar lateral diffusion of electron-hole pairs is taken into account.

Finally, this experiment also provides information on the switch-off dynamics, i.e. on the electron-hole recombination time. We observe the same behavior for both lines and obtain through the fitting procedure very similar τ_{off} time constants. For our smallest pump powers ($P \approx 1$ pJ), τ_{off} is close to 110 ps, i.e. smaller than for the 5.3 μm diameter micropillar used as an example in Fig.2. It is well known that the NRR time related to surface recombination scales as S/L for a thin semiconductor slab, where S is the surface recombination velocity and L the slab thickness[28]. One can easily show that for a cylinder of diameter D, this time scales as S/D. Taking as a reference the 200 ps value obtained for $D = 5$ μm in Fig.2, one obtains a 130 ps estimate for $D = 3$ μm. Thanks to the excellent agreement with our experimental result, we can conclude that NRR at pillar sidewalls is the dominant carrier recombination process for small pump powers. For higher pump powers, radiative recombination enters into play. Over this limited time range [30-70 ps], i.e. up

to 50 ps after the pump pulse, the decay is characterized by a smaller time constant of the order of 50 ps for the highest Ps ($P \approx 10$ pJ).

IV. ULTRAFAST TRANSIENT RECONFIGURATION OF CAVITY MODES THROUGH CAVITY SWITCHING

Differential switching, i.e. the ability to switch in different ways the modes of a cavity, has been recently observed for micropillars, using a non-uniform injection of free carriers. For instance, when free carriers are injected in a focused way close to the pillar axis, a larger switching amplitude and faster switch-on behavior is observed for *Line 1*, when compared to *Line 2*.[20] These differences can simply be explained by considering the drastically different field distributions of cavity modes: while modes related to *Line 2* have a donut shape and zero intensity on the pillar axis, mode HE_{11} has an antinode there.

Besides its size, the radial position of the focused pump spot is another useful degree of freedom. Interestingly, an off-axis injection of free carriers breaks the axial symmetry of the micropillar and is expected to lift the degeneracy of polarization-degenerate modes $HE_{\mp mn}$ and $EH_{\mp mn}$. We show in Fig.6 the result of such an experiment. We study the same 5.3 μm diameter micropillar as the one studied in Fig.2 and use a 1.1 μm diameter pump beam that is displaced about 0.9 μm to the left of the pillar axis, along the transverse x-direction.

Just after the switching pulse, we observe a splitting of *Line 2* into two branches. The splitting develops and, 5 ps after the pulse, reaches an amplitude as large as 1 meV, then decreases, and 20 ps later is no longer observable. By contrast, there is no such splitting for *Line 1*.

These experimental data are well reproduced by numerical simulations, whose results are shown by the dashed lines in Fig.6. We have already shown for an on-axis carrier injection that differential switching can be modelled accurately, provided lateral distribution of free carriers in the cavity layer of the micropillar is suitably described, taking into account the localized injection of the carriers, their lateral ambipolar diffusion and their recombination processes[20]. We follow a similar approach in the present work. We first solve Fick's law in two dimensions, taking into account diffusion and recombination processes. We assume that the refractive index change scales linearly with the density of the electron-hole plasma. Knowing the (non-circular symmetric) refractive index map at all times, we compute the

guided modes m and their effective indices $n_m^{eff}(t)$ for the 5.3 μm diameter cylinder of GaAs that forms the cavity layer of the micropillar, using a commercial software (RSOFT release 2019.09 from Synopsis). The resonance frequencies $\nu_m(t)$ of micropillar modes are then deduced at all times as[22] $\nu_{2D}/\nu_m(t) = n_m^{eff}(t)/n$. We use a single fitting parameter δn_{max}, which is the maximum refractive index change of GaAs (in absolute value), obtained at the center of the Gaussian pump spot. We obtain a very good overall agreement with our experimental data using $\delta n_{max} =$ -0.06.

In order to better understand this ultrafast transient line splitting, it is helpful to consider the field maps of the modes of the unperturbed micropillar and of the switched micropillar, shown in Fig.5. We keep in these simulations the same shape and position for the pump spot as in the experiment(1.1 μm diameter, 0.9 μm lateral displacement along x, with respect to the pillar axis z), but reduce intentionally the maximum refractive index change δn_{max} down to -0.01. According to Fig.6, this situation is representative of our experiment at the onset of the switch-on, typically 1 ps after the pulse. The index change breaks the circular symmetry, but preserves the mirror symmetry with respect to the xz-plane. Therefore, according to the perturbation theory for guided modes[29], couplings shall be induced only between modes which share the same symmetry properties. The inspection of unswitched field maps (or of the analytic expressions of modes fields for the unperturbed pillar[25]) shows that, among the four modes which contribute to *Line 2*, EH_{01} couples only with HE_{21}, while HE'_{21} only couples with HE_{01}. These couplings lead to the formation of *modes 3* to *6*, whose maps are shown in the right part of Fig.5. We see that the lowest frequency *mode 3* corresponds approximately to the sum of EH_{01} and HE_{21}. Its field intensity is close to zero on the x axis, and especially in the perturbation spot. Therefore, its frequency shifts only moderately with respect to the ones of modes EH_{01} and HE_{21}. By contrast, *mode 5* originates mainly from the difference EH_{01} - HE_{21}, whose field map has an antinode at the location of the perturbation spot. As a result, *mode 5* appears at a much higher frequency, and its field map is severely modified with respect to the one of EH_{01} - HE_{21}. Similar considerations hold for *modes 4* and *6*, and explain the splitting of *Line 2* into two branches comprising two modes each, and the observation, just after carrier injection, of a much larger switching amplitude for *modes 5* and *6* than for *modes 3* and *4*.

In marked contrast with this behavior, we do not observe any splitting of *Line 1*. Looking at the field maps of HE_{11} and HE'_{11} in Fig.5, we see that these modes do not have the same

symmetry with respect to the xz plane, and are therefore not coupled by the perturbation. Both modes experience the same blue shift, since they have very similar field intensities within the perturbed area.

Turning our attention to longer time delays (5 to 30 ps after the pulse), carrier diffusion out of the pump spot plays a dominant role. Free carriers reach regions where *modes 3-4* have a large field intensity in Fig.5; hence, diffusion induces an additional blue shift for *modes 3-4*. In the opposite way, lateral diffusion reduces the shift for *modes 5* and *6*. Hence, the splitting between the two branches decreases and vanishes once carriers are fully redistributed over the entire section of the cavity layer. After 30 ps, all modes shift back together toward their reference frequencies, due to the recombination of the free carriers.

Let us finally notice that focused off-axis switching induces a spectacular change of the field maps of the two first modes of the micropillar, as seen by comparing e.g. HE_{11} and *mode 1*. This effect, which is obtained for a small refractive index change could find interesting applications. A monochromatic emitter that is initially coupled to HE_{11}, and placed on the left side of the pump spot in Fig.5, would become decoupled from *modes 1* and *2* because of their blue-shift, and additionally because of the change of their field maps. Thanks to this combination of effects, one could likely achieve a stronger quenching of the Purcell effect, until carrier diffusion in the entire pillar restores the initial field maps of *modes 1* and *2*, i.e. during around 20 ps.

V. CONCLUSION

In this work, we have investigated ultrafast switching events induced by all-optical injection of free charge carriers in a micropillar cavity. Unlike previous work based on pump-probe spectroscopy, we are able to track with ps-time resolution all cavity modes at a time, during the entire switching event. We use a broadband internal light source, that is already active prior to the switch pulse, to funnel photons into all cavity modes present within a broad spectral band and during the entire switching event. As first results obtained with this experimental approach, we have observed very short switch-on times, down to 1.5 ps for optimum pumping conditions. We have also reported the observation of a transient splitting of one of the micropillar emission lines, which lasts for roughly 20 ps only, just after a focused and asymmetric injection of free carriers, and which results from a breaking of the

circular symmetry of the micropillar. Besides highlighting some key assets of this characterization method, our results pave the way to a more systematic exploration of switching events, and noticeably of transient reconfigurations of the set of resonant cavity modes, in micropillars as well as in more sophisticated photonic systems such as photonic molecules[15] or coupled cavities, which are particularly attractive for the dynamic control of the emission of a single quantum emitter[11,30]. Beyond their fundamental interest, such transient changes of the modal structure could also be useful to switch the emission of embedded emitters from one mode to another, and achieve e.g. ultrafast beam steering or (when applied to cavities containing a single QD) superposition states of a single photon shared by two modes.

ACKNOWLEDGMENTS

The authors would like to thank W.L. Vos for numerous discussions and insightful advice. This paper is based on work supported by the French National Agency of Research (ANR) under the contract NOMOS (ANR-18- CE24-0026). G.M.T. and P.L.S. acknowledge funding from CAPES (PDSE 88881.187056 /2018.1) and CNPq.

The data that support the findings of this study are available from the corresponding author upon reasonable request.

REFERENCES

[1]J. L. Jewell, A. Scherer, S. L. M. Call, A. C. Gossard, and J. H. English, Appl. Phys. Lett. **51**, 94 (1987).

[2]R. Kuszelewicz, J.L.Oudar, J.C.Michel, and R.Azoulay, Appl. Phys. Lett. **53**, 2138 (1988).

[3]Q. Xu, B. Schmidt, S. Pradhan, and M. Lipson, Nature **435**, 325 (2005).

[4]E. Yüce, G. Csistis, J. Claudon, E. Dupuy, R. Nuijs, B. de Ronde, A.P.Mosk, J.M.Gérard, and W.L.Vos, Opt. Lett. **38**, 374 (2013).

[5]P.J.Harding, T. Euser, Y. Nowicki-Bringuier, J.M.Gérard, and W.L.Vos, Appl. Phys. Lett. **91**, 111103 (2007).

[6]K. Nozaki, T. Tanabe, A. Shinya, T. Sato, H. Taniyama, and M. Notomi, Nat. Photon. **4**, 477 (2010).

[7]C. Husko, A. DeRossi, S. Combrié, Q. Tran, F. Raineri, and C. Wong, Appl. Phys. Lett. **94**, 021111 (2009).

[8]P. Colman, P. Lunnemann, Y. Yu, and J. Mork, Phys. Rev. Lett. **117**, 233901 (2016).

[9]I. Fushman, E. Waks, D. Englund, N. Stoltz, P. Petroff, and J. Vuckovic, Appl. Phys. Lett. **90**, 091118 (2007).

[10]H. Thyrrestrup, A. Hartsuiker, J.M.Gérard, and W.L.Vos, Opt. Exp. **21**, 23130 (2013).

[11]C.Y.Jin, R.Johne, M.Y.Swinkels, T.B.Hoang, L.Midolo, P. Veldhoven, and A. Fiore, Nat. Nanotech. **9**, 886 (2014).

[12]G.Hornecker, E.Peinke, J.Claudon, A.Auffèves, and J.M.Gérard, Proc. SPIE **9505**, DOI 10.1117/12.2178991 (2015).

[13]S. Preble, Q.Xu, and M. Lipson, Nat. Photon. **1**, 293 (2007).

[14]J.M.Gérard, B. Sermage, B. Gayral, B. Legrand, E. Costard, and V. Thierry-Mieg, Phys. Rev. Lett. **81**, 1110 (1998).

[15]S.Reitzenstein and A.Forchel, J. Phys.D:Appl.Phys. **43**, 033001 (2010).

[16]E.Moreau, I.Robert, J.M.Gérard, I.Abram, L.Manin, and V.Thierry-Mieg, Appl. Phys. Lett. **79**, 2865 (2001).

[17]O.Gazzano, S. de Vasconcellos, C.Arnold, A.Nowak, E.Galopin, I.Sagnes, L.Lanco, A.Lemaître, and P.Senellart, Nat. Commun. **4**, 1425 (2013).

[18]X.Ding, Y. He, Z.C.Duan, N.Gregersen, M.C.Chen, S.Unsleber, S.Maier, C.Schneider, M.Kamp, S.Höfling, C.Y.Liu, and J.W.Pan, Phys. Rev. Lett. **116**, 020401 (2012).

[19]C.Arnold, V. Loo, A. Lemaître, I. Sagnes, O. Krebs, P. Voisin, P. Senellart, and L. Lanco, Appl. Phys. Lett. **100**, 111111 (2012).

[20]H. Thyrrestrup, E. Yüce, G. Ctistis, J. Claudon, W.L.Vos, and J.M.Gérard, Appl. Phys. Lett. **105**, 111115 (2014).

[21]T.Rivera, J.P.Debray, J.M.Gérard, B.Legrand, L.Manin, and J.L.Oudar, Appl. Phys. Lett. **74**, 911 (1999).

[22]J.M.Gérard, D.Barrier, J.Y.Marzin, R.Kuszelewicz, L.Manin, E.Costard, V.Thierry-Mieg, and T.Rivera, Appl. Phys. Lett. **69**, 449 (1996).

[23]E.Viasnoff-Schwoob, C.Weisbuch, H.Benisty, S.Olivier, S.Varoutsis, I.Robert-Philip, R.Houdré, and C.J.M.Smith, Phys. Rev. Lett. **95**, 183901 (2005).

[24]T. Sattler, E. Peinke, J. Bleuse, J. Claudon, W.L.Vos, and J.M.Gérard, IEEE Book series, Proc. 19th Int. Conf. on Transparent Optical Networks , DOI 10.1109/IC-

TON.2017.8025177 (2017).

[25]A.Yariv, "Optical electronics," (Saunders College, San Francisco, 1991).

[26]B.R.Bennett, R.A.Soref, and J.A.DelAlamo, IEEE J. Quantum. Electron. **26**, 113 (1990).

[27]J.L.Oudar, D.Hulin, A.Migus, A.Antonetti, and F.Alexandre, Phys. Rev. Lett. **55**, 2074 (1985).

[28]E.Yablonovitch, T.J.Gmitter, and R.Bhat, Phys. Rev. Lett. **61**, 2546 (1988).

[29]C.Vassalo, "Optical waveguide concepts," (Amsterdam, 1991).

[30]D. Pellegrino, F. Pagliano, A. Genco, M. Petruzella, F. vanOtten, and A. Fiore, Appl. Phys. Lett. **112**, 161110 (2018).

VI. LIST OF FIGURE CAPTIONS

FIG.1. Schematic of the time-resolved microphotoluminescence set-up used in this work. Green curved lines represent optical fibers. The micropillar cavity is placed in a He-cooled cryostat working at 4K.

FIG.2. Streak camera image obtained for a 5.3 μm diameter switched QD-micropillar, showing the temporal evolution of its six lowest frequency emission lines under uniform free carrier injection. Colors correspond to the linear intensity scale shown on the right. Each emission line is labelled by listing on its left side the resonant pillar modes which contribute to it. Here $\gamma = 0.9$, $\Delta = 90$ ps, $E_{pump} = 1.57$ eV. The switching pulse energy is around 5 pJ. A bi-exponential fit of the time-dependence of the mode frequency is shown as a black line for the fundamental mode HE_{11}. Other colored lines are obtained by performing a translation of this curve, so as to highlight the similarity of the switching behavior for all modes that results from the uniform injection of free carriers in this experiment.

FIG.3. Streak camera images obtained for a 3 μm diameter micropillar for $\gamma = 0.5$, $\Delta = 200$ ps and $E_{pump} = 1.55$ eV. The switching pulse energy is $P = 0.5$ pJ (top) and 7 pJ (bottom). The black dashed line marks the arrival time of the switching pulse. Blue lines mark the central position of the emission lines. Green lines correspond to the best fitting curves, obtained from the simple procedure described in the text.

FIG.4. Dependence of the switch-on time τ_{on} (top) and switch-off time τ_{off} (bottom) as a function of the switching pulse energy P, for the two first sets of modes of a 3 μm diameter micropillar ($\gamma = 0.5$, Δ =200 ps and $E_{pump} = 1.57$ eV).

FIG. 5. Vectorial maps of the in-plane electric field and of the field intensity for the six lowest frequency modes of a 5.3 μm diameter micropillar. The linear color scale is normalized to one at maximum for each map, and the black circle marks the position of the edge of the micropillar. Left: maps for the unswitched micropillar. Right: maps obtained after switching with a pump pulse that is focused off-axis at the location marked by the white circle (Gaussian profile, 1.1 μm diameter at half-maximum, 0.9 μm shift to the left of to the pillar axis). We assume that the maximum refractive index change, obtained at the center of the spot, is $\delta n_{max} = -0.01$. For the switched micropillar, circular symmetry is broken; modes are then simply labelled in increasing frequency order.

FIG. 6. Streak camera image obtained for a 5.3 μm diameter micropillar excited by a focused off-axis pump beam. Here, $\gamma = 0.5$, $\Delta = 1.1$ ns, $E_{pump} = 1.55$ eV, $P = 10$ pJ. The Gaussian pump beam has a 1.1 μm diameter at waist and is focused 0.9 μm away from the center of the micropillar top facet. The dashed lines correspond to the calculated mode frequencies, resulting from a model taking into account carrier injection, lateral diffusion and recombination.

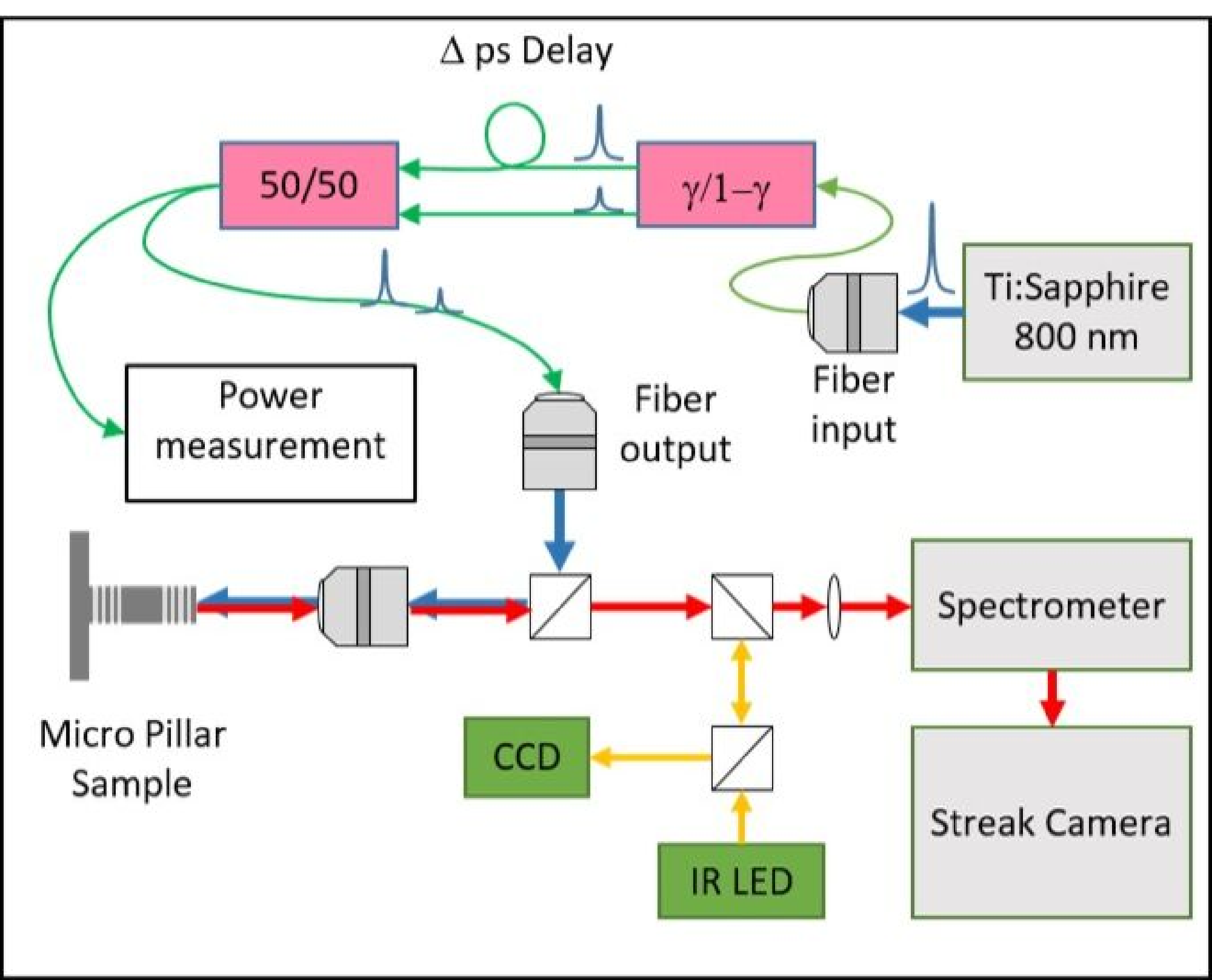
Δ ps Delay
50/50
γ/1−γ
Ti:Sapphire
800 nm
Fiber
input
Power
measurement
Fiber
output
Spectrometer
Micro Pillar
Sample
CCD
IR LED
Streak Camera

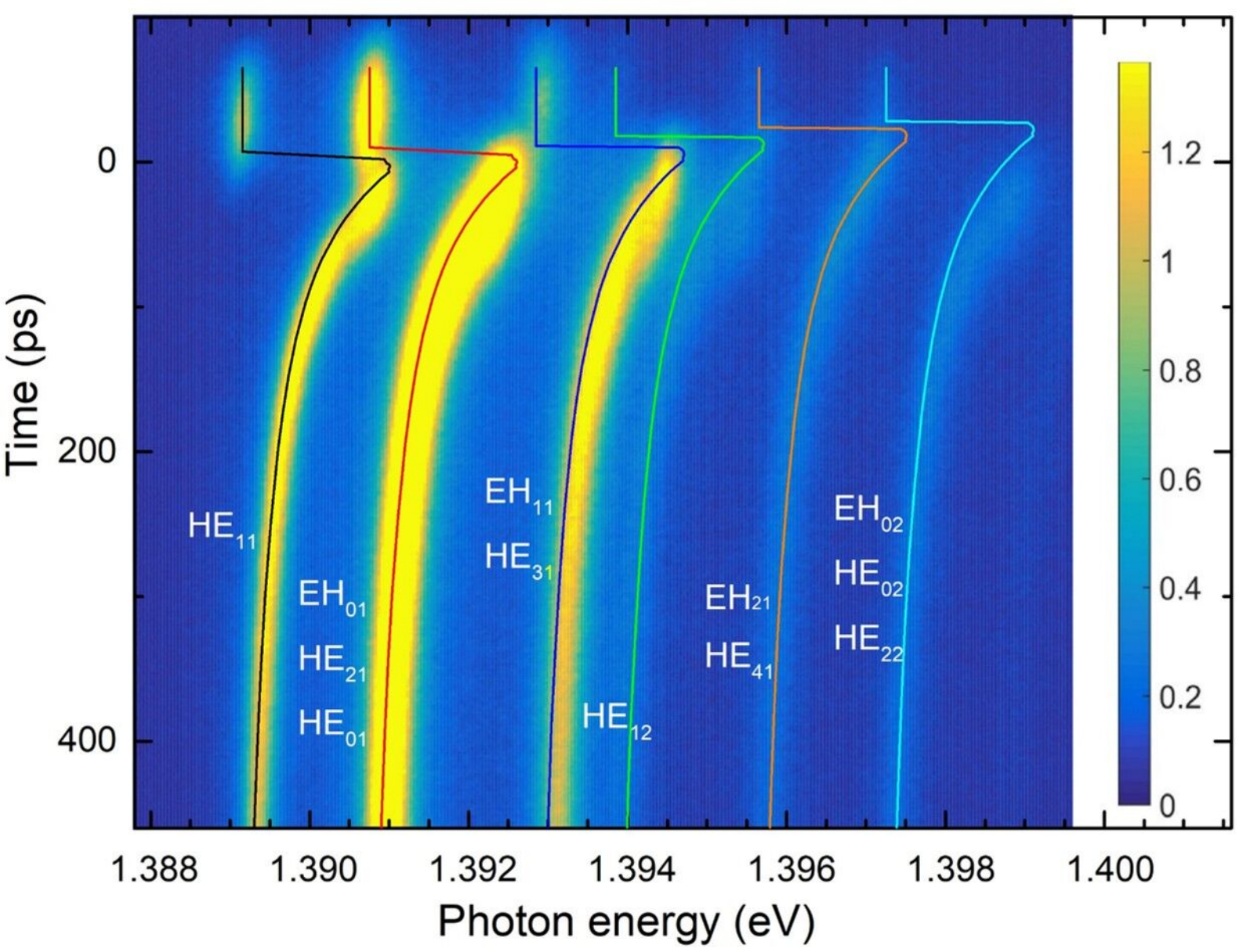
Time (ps)
0
200
400
HE11
EH01
HE21
HE01
EH11
HE31
HE12
EH21
HE41
EH02
HE02
HE22
1.2
1
0.8
0.6
0.4
0.2
0
1.388
1.390
1.392
1.394
1.396
1.398
1.400
Photon energy (eV)

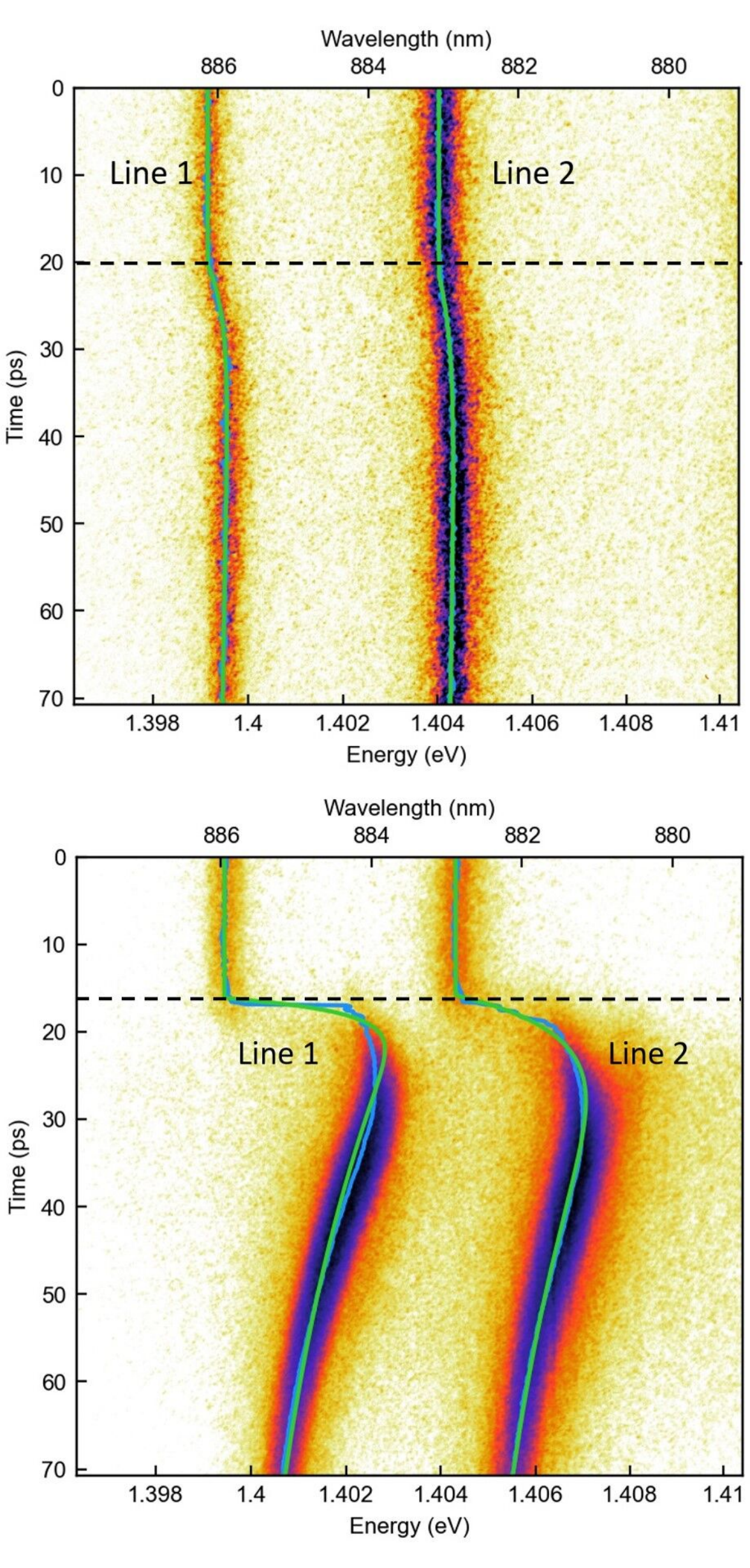
Wavelength (nm)
886
884
882
880
Line 1
Line 2
Time (ps)
0
10
20
30
40
50
60
70
1.398
1.4
1.402
1.404
1.406
1.408
1.41
Energy (eV)
Wavelength (nm)
886
884
882
880
Line 1
Line 2
Time (ps)
0
10
20
30
40
50
60
70
1.398
1.4
1.402
1.404
1.406
1.408
1.41
Energy (eV)

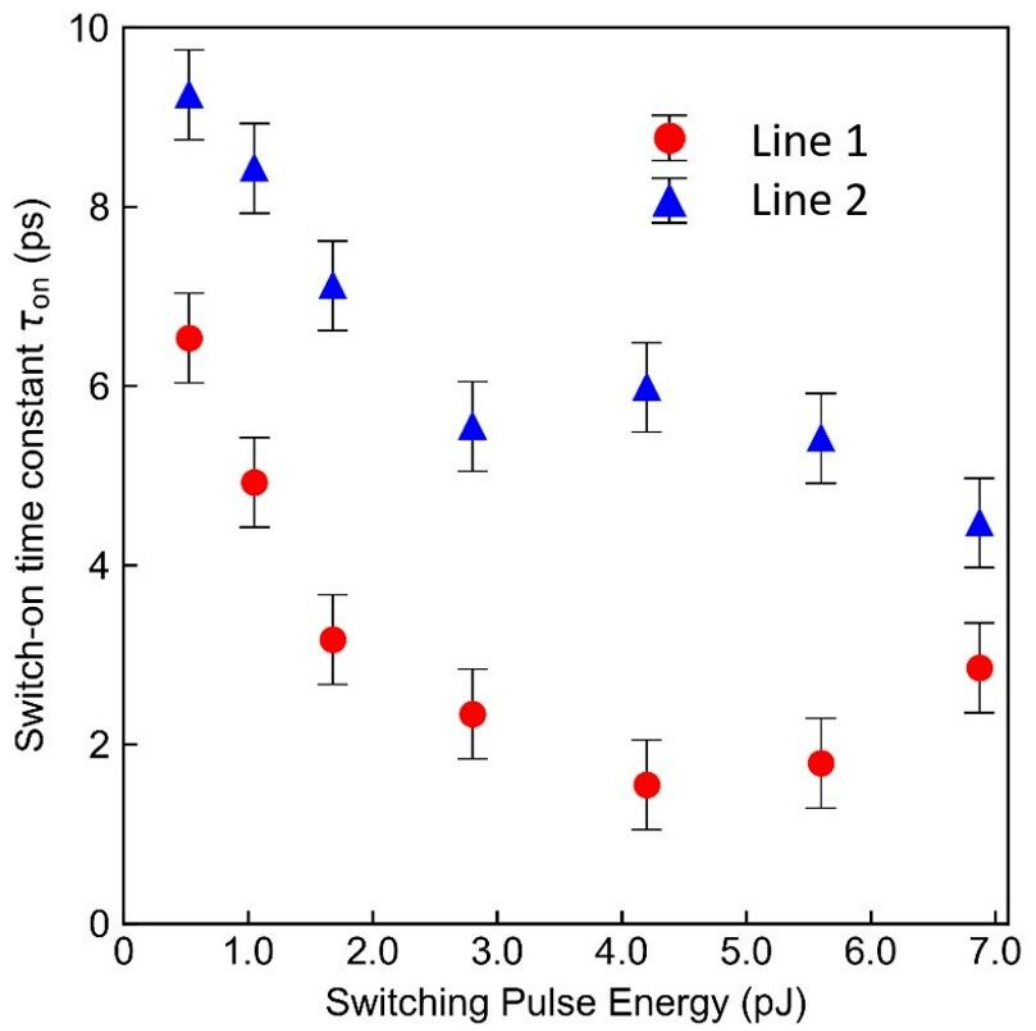
Switch-on time constant τ_{on} (ps)
Switching Pulse Energy (pJ)
Line 1
Line 2
0
2
4
6
8
10
0
1.0
2.0
3.0
4.0
5.0
6.0
7.0

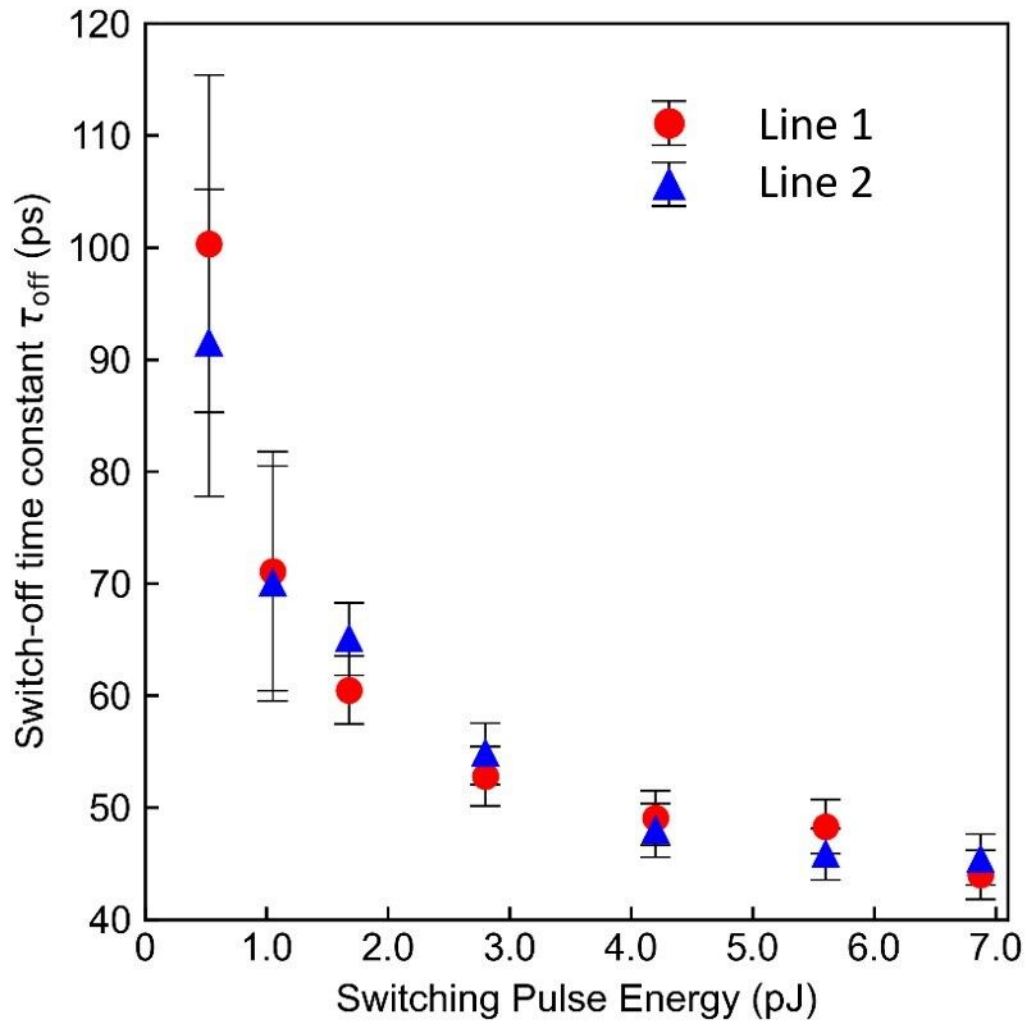
Switch-off time constant τ_{off} (ps)
Switching Pulse Energy (pJ)
Line 1
Line 2
40
50
60
70
80
90
100
110
120
0
1.0
2.0
3.0
4.0
5.0
6.0
7.0

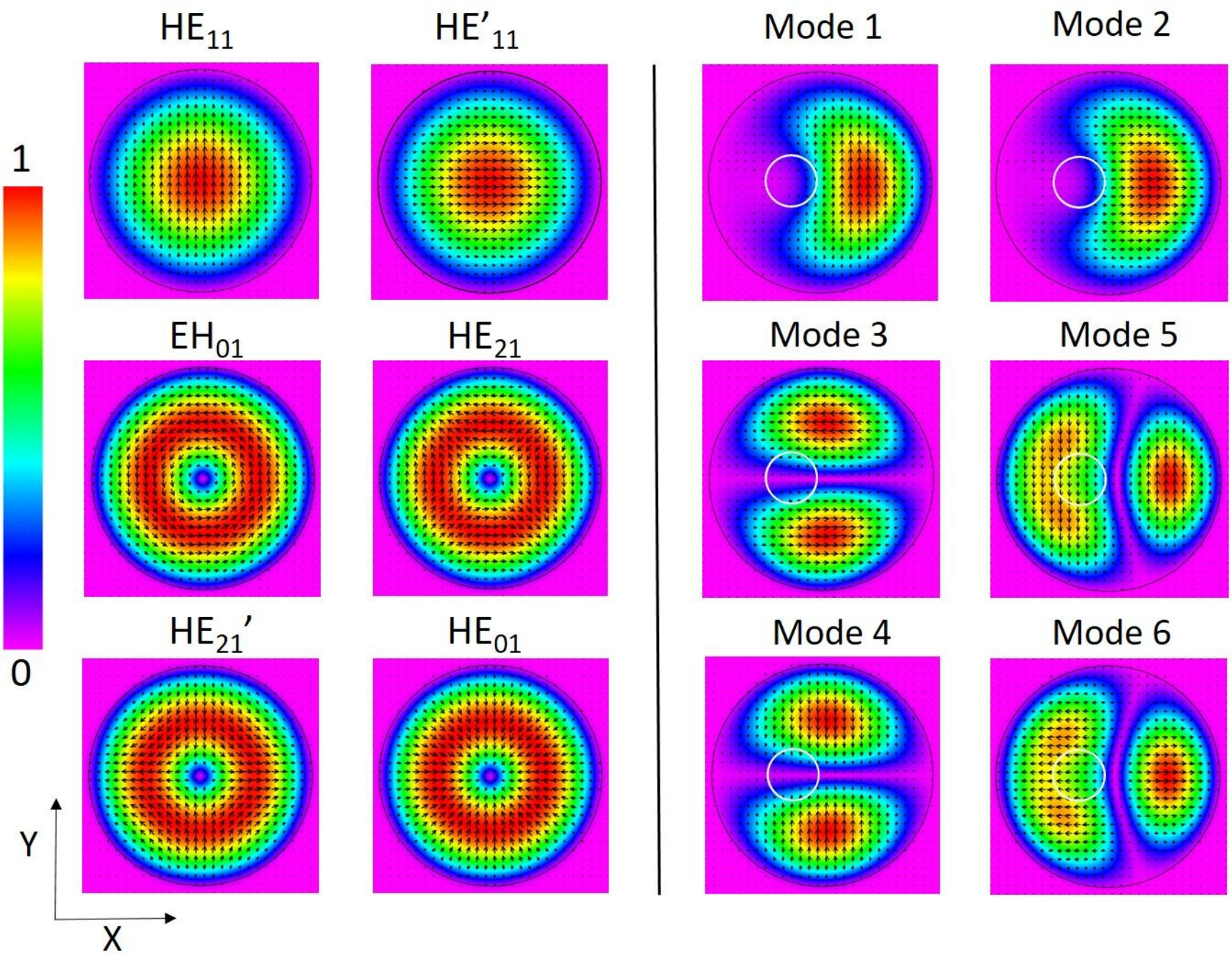
HE11
HE'11
Mode 1
Mode 2
1
EH01
HE21
Mode 3
Mode 5
HE21'
HE01
Mode 4
Mode 6
0
Y
X

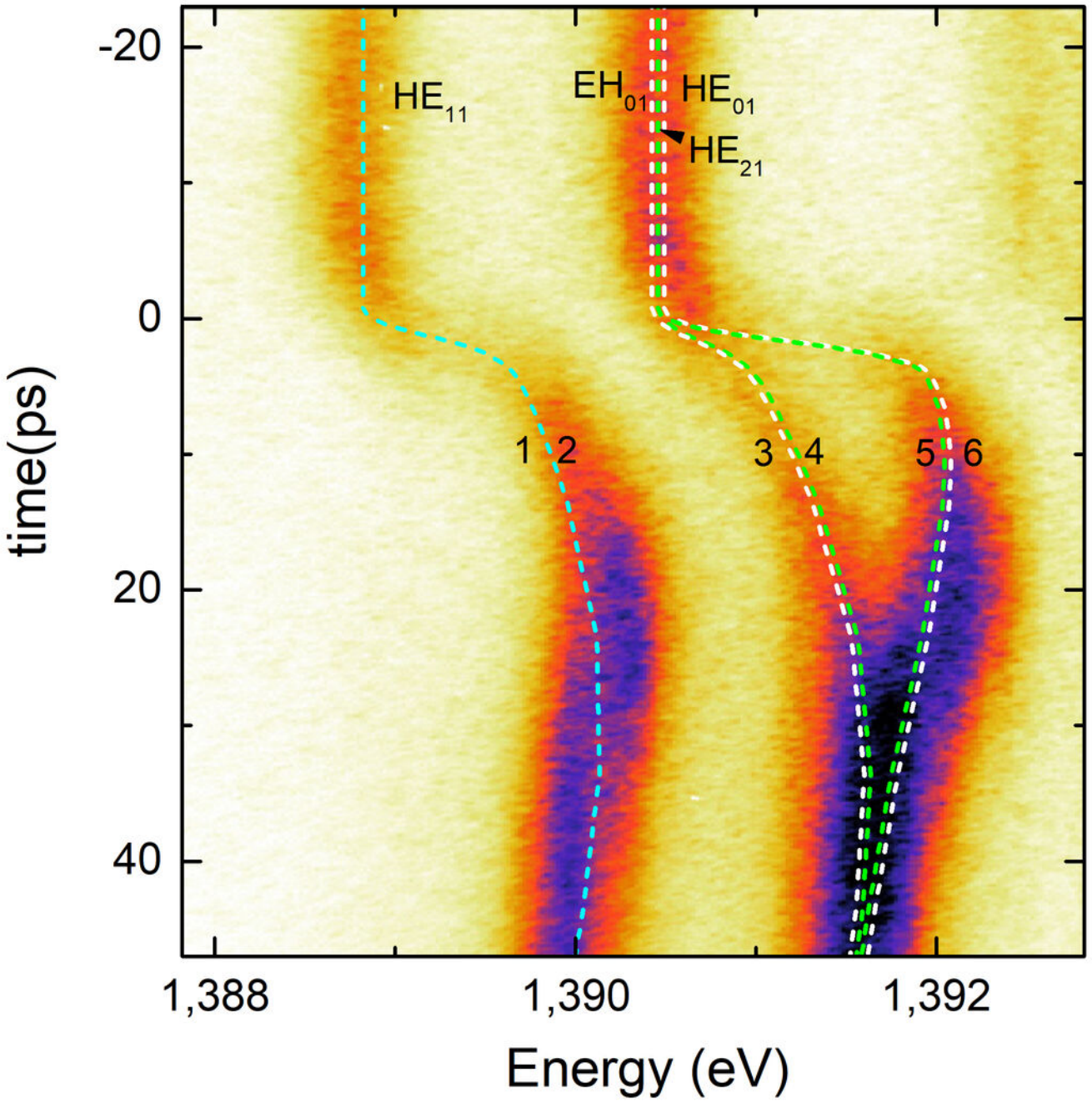
-20
0
20
40
time(ps)
HE11
EH01
HE01
HE21
1
2
3
4
5
6
1,388
1,390
1,392
Energy (eV)